Correlation Model for Turbulence along the Glide Path

Lloyd D. Reid*
University of Toronto, Institute for Aerospace Studies, Toronto, Ontario

Flight through the earth's planetary boundary layer can result in wind shear and turbulence inputs to an aircraft that adversely affect its performance of the landing approach maneuver. A turbulence correlation technique has been developed to predict these effects for a range of flight vehicles including the particularly demanding situations involving VTOL and STOL aircraft. In the present study, the required turbulence correlations were obtained in an experimental program carried out in a planetary boundary-layer wind tunnel. Using these measurements and a modified von Kármán turbulence correlation model, the longitudinal response of a light STOL transport was predicted for a range of conditions to assess the performance of the method. It was found that the turbulence correlation technique produced reasonable estimates of the rms response of the aircraft's state vector to planetary boundary-layer turbulence and that, if some sacrifice in precision was accepted, a considerable reduction in the number of experimental measurements required could be achieved. The sensitivity of the results to the shape of the correlation curves was also studied and found to be acceptable.

Nomenclature

$F_B;F_I;F_T$	= reference frames: stability axes; earth-fixed; wind tunnel
F	= external force applied to the aircraft
$\mathcal{G}_i$	= turbulence components in F_T; two components when $i=t$ and three when $i=T$
h	= height above ground level
$\boldsymbol{h}$	= aircraft angular momentum about mass center
$\mathcal{H}(t,t')$	= aircraft impulsive response matrix
L_u^x, L_w^x	= longitudinal and lateral turbulence scale
m	= aircraft mass
M	= external moment applied about the aircraft center of mass
q	= pitch rate in frame F_B
$\mathcal{R}$	= turbulence correlation matrix
t	= time, s
t_i	= time for aircraft to reach ith probe
(uvw)	= components of V in F_B, or turbulence components in F_T depending on context
V	= airspeed
V_E	= groundspeed
W	= windspeed, or mean wind depending on context
x_I	= x coordinate of aircraft in F_I
γ_E	= glide slope angle
$\Delta(\cdot)$	= a perturbation about the reference equilibrium value
Δu_c	= $(\Delta\eta\Delta\pi)^T$, control input
$\Delta W_1, \Delta W_2$	= x and z direction turbulence components in F_I
$\Delta\mathfrak{x}$	= $(\Delta u\Delta w\Delta q\Delta\theta\Delta x_I\Delta h)^T$ matrix of state variable perturbations
Δ_z	= intermediate variable in solution for $\Delta\mathfrak{x}$
$\Delta\eta$	= elevator angle perturbation
$\Delta\theta$	= Euler elevation angle perturbation
$\Delta\pi$	= throttle setting perturbation
τ	= time delay, s
X	= a vector with components $\mathfrak{X}$ in a specified reference frame
$\mathfrak{X}$	= a matrix
$\mathfrak{X}^T$	= transpose of $\mathfrak{X}$
$\dot{X}$	= $\dfrac{dX}{dt}$ as seen from F_I
$\hat{x}$	= $\sqrt{\langle x^2\rangle}$
$\langle x\rangle$	= expected value of x
$\bar{x}$	= time average of $x(t)$
$(\cdot)_e$	= reference equilibrium value
$(\cdot)_G$	= value at the top of the earth's boundary layer

Received June 27, 1977; revision received Sept. 26, 1977.

Index categories: Landing Dynamics; Atmospheric and Space Sciences.

*Associate Professor, Institute for Aerospace Studies. Associate Fellow AIAA.

Introduction

THE work presented here represents the next step in a sequence of theoretical developments and experimental measurements begun as outlined in Ref. 1. It is aimed at predicting the response of aircraft to turbulence during the landing approach through the earth's planetary boundary layer. This task is particularly challenging to study because the turbulence input as seen by the aircraft performing the landing approach is a nonstationary process and the turbulence field in the earth's boundary layer is both inhomogeneous and nonisotropic. These factors point out the need to perform a time-domain analysis, which includes the effects of the vehicle's transient response and the nonstationary nature of the input. Past studies based on power spectral density techniques[2,3] have often either omitted some of these effects or employed approximations to them. (In Ref. 4 a comparison between the turbulence correlation technique and these other techniques indicates that significant errors can be introduced by not including these effects.)

The basis of the present method is the application of two-point space/time correlations among the turbulence velocity components (herein called turbulence correlations) as measured along the glide slope. A full description of this is given in Refs. 1 and 5. The advantages of this technique are its ability to handle the transient response of the aircraft as it enters the boundary layer, its representation of the nonstationary nature of the turbulence inputs to the aircraft as it proceeds down the glide slope, and the fairly straightforward fixed-probe experimental measurements employed in determining the turbulence correlation matrix. Thus fewer assumptions than used in the past need be made in the analysis of aircraft response to turbulence during the landing approach. In addition, a unique feature of the turbulence correlation technique is its ability to predict aircraft response in situations where the presence of terrain features and manmade structures near the runway generate unusual wind shear and turbulence. Therefore, this technique (coupled with suitable wind tunnel or field measurements) can handle such

problems as downtown STOLport site evaluations and the study of the flight safety implications of unusual wind conditions near currently operational runways. Its inherent limitations are the need to represent the aircraft by a linearized set of equations and the fact that the predicted response is in the form of rms dispersions about a reference equilibrium flight condition, with no indication of the underlying distribution function (which must be determined by other means).

In the present paper, the turbulence correlation technique is extended to allow the analysis of a generalized form of the aircraft equations of motion. An investigation is then carried out to determine the suitability of a modified form of von Kármán's model for atmospheric turbulence correlations for fitting experimental correlation measurements made in the new UTIAS 44×66 in., jet-driven, planetary boundary-layer wind tunnel. It is hoped that such models will reduce the number of wind tunnel or field measurements required in applying the turbulence correlation method. Finally, a simplified model of a light STOL transport is employed to demonstrate the application of the turbulence correlation technique.

Linearized Aircraft Motion Equations

To apply the turbulence correlation technique, it is necessary to develop a linearized set of equations of motion for the aircraft flying in the presence of wind shear and turbulence. The nonlinear motion equations can be written as

$$m(\dot{V}+\dot{W})=F \tag{1}$$

$$\dot{h}=M \tag{2}$$

$$V_E=V+W \tag{3}$$

In the present case the simplest approach to linearizing these equations is to select a reference equilibrium flight condition corresponding to a constant airspeed (V_e) landing approach along a rectilinear glideslope of angle γ_E with respect to the horizontal in the presence of a constant headwind (W_e). Perturbations in the aircraft's state vector away from the reference equilibrium are then treated as arising from initial conditions, wind-shear effects, turbulence, and control inputs. Because the equations are linear, the response to their combined effects can be found by computing the response to each in isolation and then summing together the results.

The resulting longitudinal equations are obtained by following the standard approach employed in Ref. 6 with the addition of the point approximation whereby the physical size of the aircraft is considered to be smaller than typical wavelengths in the turbulence field.

When written as components in the body-fixed stability axes frame F_B, the perturbation equations are

$$\Delta\dot{\alpha}=\mathcal{A}\Delta\alpha+\mathcal{C}_1\Delta u_c+\mathcal{C}_2\Delta\mathcal{W}+\mathcal{C}_3\Delta\dot{\mathcal{W}} \tag{4}$$

$$\Delta\alpha^T=(\Delta u\,\Delta w\,\Delta q\,\Delta\theta\,\Delta x_1\,\Delta h) \tag{5}$$

$$\Delta u_c{}^T=(\Delta\eta\,\Delta\pi) \tag{6}$$

$$\Delta\mathcal{W}^T=(\Delta W_1\,\Delta W_3) \tag{7}$$

In the present case $\mathcal{A}$, $\mathcal{C}_1$, $\mathcal{C}_2$, and $\mathcal{C}_3$ are constant matrices. Here, since only the response to turbulence is sought, ΔW_1 and ΔW_3 are taken to represent the x and z turbulence components in F_1 (see Fig. 1). The above equations reduce to the standard form of Ref. 6 when $\Delta\mathcal{W}$ is set identically equal to zero. (See Ref. 4 for a full development.)

Because $\Delta\dot{\mathcal{W}}$ was not measured in the wind tunnel program, it is necessary to rewrite Eq. (4) to remove it as an explicit term. This is done by introducing an intermediate variable Δz where

$$\Delta\alpha=\Delta z+\mathcal{C}_3\Delta\mathcal{W} \tag{8}$$

Substituting Eq. (8) into Eq. (4), it is found that

$$\Delta\dot{z}=\mathcal{A}\Delta z+\mathcal{C}_1\Delta u_c+(\mathcal{C}_2+\mathcal{A}\mathcal{C}_3)\Delta\mathcal{W} \tag{9}$$

Equations (8) and (9) can then be solved for $\Delta\alpha$.

Computation of Aircraft Response to Turbulence Based on Turbulence Correlations

The theoretical basis for this technique is outlined in Refs. 1 and 5 for the case where $\Delta\dot{\mathcal{W}}$ is absent from Eq. (4). In this section, the development is expanded to include $\Delta\dot{\mathcal{W}}$ effects.

Because this theory is to be applied to wind tunnel data, it makes sense to write Eqs. (8) and (9) in terms of turbulence velocity components in the wind tunnel frame F_T (see Fig. 1). A slight notation problem arises because it is common practice to use $\mathcal{g}_T^T=(u,v,w)$ where u, v, and w represent the x, y, and z components of turbulence in F_T. In general the context will indicate whether u, v, and w represent turbulence velocity components in F_T or aircraft airspeed components in the stability axes frame F_B. From Fig. 1 it is seen that

$$\Delta\mathcal{W}=-\mathcal{g}_t \tag{10}$$

where

$$\mathcal{g}_t=\begin{bmatrix}1&0&0\\0&0&1\end{bmatrix}\mathcal{g}_T \tag{11}$$

Anticipating that the analysis is to be performed in this paper will consider turbulence inputs only, Eq. (10) is substituted into Eqs. (8) and (9) with $\Delta u_c=0$ to produce

$$\Delta\dot{z}=\mathcal{A}\Delta z-(\mathcal{C}_2+\mathcal{A}\mathcal{C}_3)\mathcal{g}_t \tag{12}$$

$$\Delta\alpha=\Delta z-\mathcal{C}_3\mathcal{g}_t \tag{13}$$

where $\Delta\alpha$ now represents the response to turbulence alone.

Starting with Eqs. (12) and (13) it is desired to find at some time t

$$\begin{aligned}\langle\Delta\alpha(t)\Delta\alpha^T(t)\rangle&=\langle(\Delta z-\mathcal{C}_3\mathcal{g}_t)(\Delta z-\mathcal{C}_3\mathcal{g}_t)^T\rangle\\&=\langle\Delta z\Delta z^T\rangle\\&+\mathcal{C}_3\langle\mathcal{g}_t\mathcal{g}_t^T\rangle\mathcal{C}_3^T\\&-\mathcal{C}_3\langle\mathcal{g}_t\Delta z^T\rangle\\&-(\mathcal{C}_3\langle\mathcal{g}_t\Delta z^T\rangle)^T\end{aligned} \tag{14}$$

Following the approach taken in Refs. 1 and 5, it can be shown that

$$\langle\Delta z\Delta z^T\rangle=\int_0^t\int_0^t\mathcal{H}(t,t_1)\mathcal{R}(t_1,t_2)\mathcal{H}^T(t,t_2)\,dt_1\,dt_2 \tag{15}$$

where

$$\mathcal{H}(t,t')=[\exp\{(t-t')\mathcal{A}\}][-(\mathcal{C}_2+\mathcal{A}\mathcal{C}_3)] \tag{16}$$

is the impulsive response matrix of the system represented by Eq. (12). $\mathcal{R}(t_1,t_2)$ is the turbulence correlation matrix defined as

$$\mathcal{R}(t_1,t_2)=\langle\mathcal{g}_i(t_1)\mathcal{g}_i^T(t_2)\rangle \tag{17}$$

where $\mathcal{R}$ is 3×3 when $i=T$ and $\mathcal{R}$ is 2×2 when $i=t$ (the context will generally indicate the dimension of the matrix) and $\mathcal{g}_i(t)$ represents the turbulence input to the aircraft at time t. The ijth element of $\mathcal{R}(t_1,t_2)$ is $\langle u_i(t_1)\, u_j(t_2)\rangle$ where $u_1=u$, $u_2=v$ and $u_3=w$. These turbulence correlations can be measured by using two stationary velocity probes fixed at pairs of points along the specified glide slope. The second-order effect caused by the fact that the aircraft itself will be slightly perturbed away from the glide slope is ignored in this development. Assuming ergodicity, it then follows that

$$\mathcal{R}(t_1,t_2)=\overline{\mathcal{g}_i(r_1,t)\,\mathcal{g}_i^T(r_2,t+\tau)} \tag{18}$$

where

$$\tau=t_2-t_1 \tag{19}$$

and $\mathcal{g}_i(r_j,t)$ represents the time history of the turbulence as measured at the location on the glide slope (given by r_j), which is reached by the aircraft at time t_j.

The term $\langle \mathcal{g}_t \mathcal{g}_t^T\rangle$ in Eq. (14) is simply $\mathcal{R}(t,t)$. The other expression that must be evaluated is $\langle \mathcal{g}_t \Delta_z{}^T\rangle$. Following an approach similar to that used in Refs. 1 and 5 to develop Eq. (15) it can be shown that

$$\langle \mathcal{g}_t \Delta_z{}^T\rangle=\int_0^t \mathcal{R}(t,t')\,\mathcal{H}^T(t,t')\,dt' \tag{20}$$

Thus Eq. (14) becomes

$$\begin{aligned}\langle \Delta_x(t)\Delta_x{}^T(t)\rangle &= \int_0^t\int_0^t \mathcal{H}(t,t_1)\,\mathcal{R}(t_1,t_2)\,\mathcal{H}^T(t,t_2)\,dt_1\,dt_2\\ &+\mathcal{C}_3\,\mathcal{R}(t,t)\,\mathcal{C}_3^T\\ &-\mathcal{C}_3\int_0^t \mathcal{R}(t,t')\,\mathcal{H}^T(t,t')\,dt'\\ &-\left(\mathcal{C}_3\int_0^t \mathcal{R}(t,t')\,\mathcal{H}^T(t,t')\,dt'\right)^T\end{aligned} \tag{21}$$

Note that the diagonal of $\langle \Delta_x(t)\Delta_x{}^T(t)\rangle$ gives the mean square of the state variable perturbations.

Since no analytic model existed for $\mathcal{R}$, it was necessary to measure the flight path correlations in the wind tunnel. The evaluation of Eq. (21) has been implemented on a digital computer for an aircraft with parameters based on specified reference equilibrium conditions.

Turbulence Correlation Measurements

The turbulence correlation measurements were made in a wind tunnel (with a cross section of 44×66 in.) set up to model a planetary boundary layer with a mean wind profile W given by

$$W/W_G=(h/h_G)^{0.16} \tag{22}$$

with $W_G=66$ fps and $h_G=1000$ ft. The flow properties were adjusted to represent conditions that might exist over smooth open terrain under neutral atmospheric conditions in the presence of a strong wind. The grid of velocity probe locations included seven upper probe locations with eight lower probe locations used for each. The details of the wind tunnel simulation and the turbulence correlation measurement program are presented fully in Ref. 5. Figures 1 to 3 summarize the gross features of the simulated flow (note that L_u^x and L_w^x are the longitudinal and lateral turbulence scales, respectively) and Figs. 4-8 give some typical results for $\mathcal{R}$. The turbulent scales are measures of the spatial extent of significant turbulence correlation. Following the terminology of Ref. 5, the term longitudinal (lateral) refers to the spatial

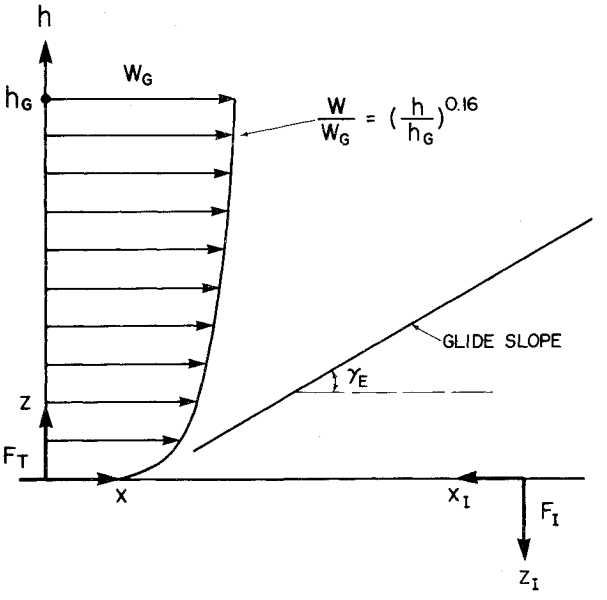

Fig. 1 Mean wind profile and glide slope.

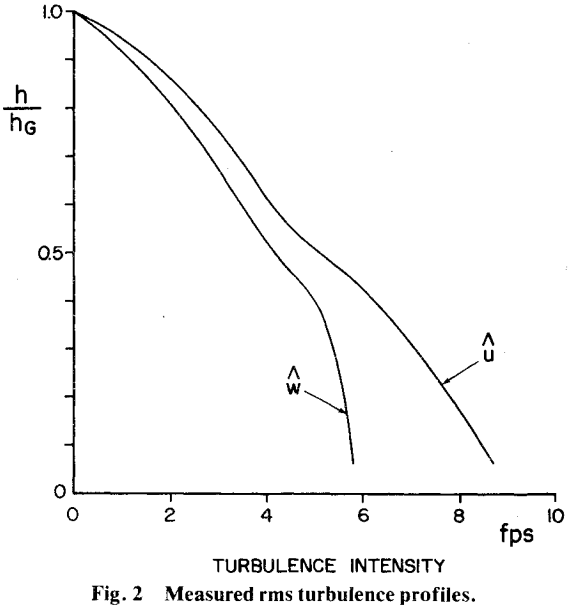

Fig. 2 Measured rms turbulence profiles.

axis being parallel (orthogonal) to the direction of the pertinent turbulence velocity component. The latter plots are nondimensionalized to produce $\tilde{\mathcal{R}}$ by dividing by the product of the rms of the turbulence velocities as measured at the two probe locations. In this case a 15-deg rectilinear glide slope has been assumed and the measurements made along this path using constant-temperature hot-wire anemometers. (This value of $\gamma_E=15$ deg was selected because it was felt to be sufficiently large to represent future STOL trends yet still within the current state-of-the-art.) Here t_1 represents the time taken by the aircraft to reach the upper probe location from a starting point near the top of the boundary layer and t_2 the same for the lower probe location. Seven upper probe locations were utilized ranging from a full-scale height of $h_1=694$ ft down to $h_1=140$ ft. It is seen that plotting the data in this manner collapses them to a considerably degree. Data measurements were made for V_e/W_G ratios of 1.5 and 2.0.

Model Fits to the Turbulence Correlation Data

At the present time, no analytical model exists for predicting cross-correlations among turbulence velocity components in the planetary boundary layer. As a first step in

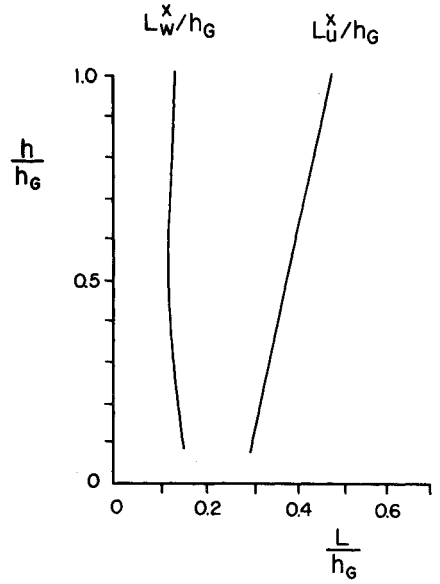

Fig. 3 Measured turbulence scale profiles.

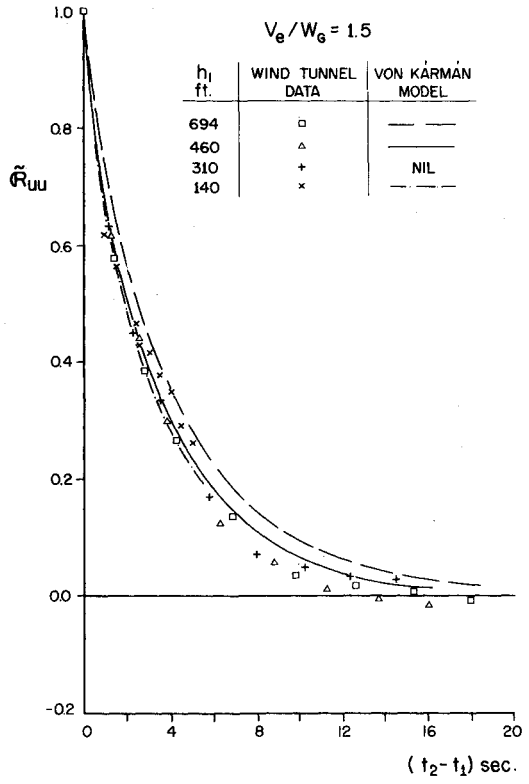

Fig. 4 Comparison between wind tunnel correlation measurements and the von Kármán model.

describing these features it was decided to apply a modified version of a model developed for homogeneous, isotropic turbulence. Based on preliminary comparisons with the wind tunnel generated $\tilde{\mathfrak{R}}$ data it was felt that the von Kármán model (based on homogeneous, isotropic, Gaussian, and frozen flow) might form a reasonable basis for fitting the test results. The von Kármán model has the form (see for example Ref. 6):

$$\tilde{R}_{ij}(\xi_1,\xi_2,\xi_3) = [f(\zeta)-g(\zeta)]\,(\xi_i\xi_j/\xi^2)+g(\zeta)\delta_{ij} \tag{23}$$

where

i or $j=1$ represents the x direction
i or $j=2$ represents the y direction
i or $j=3$ represents the z direction

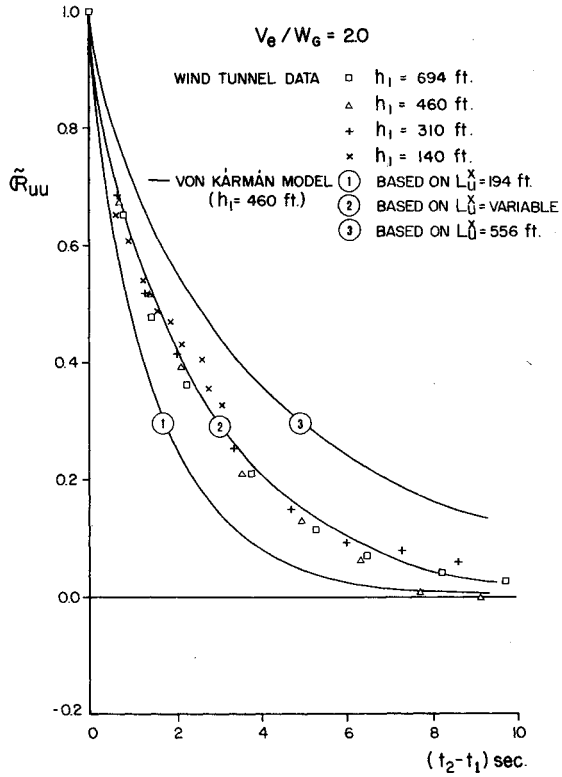

Fig. 5 Turbulence correlation $\tilde{\mathfrak{R}}_{uu}$.

$\tilde{R}_{ij}(\xi_1,\xi_2,\xi_3)$ represents the correlation between the ith turbulent component at (xyz) in F_T and the jth turbulent component at $(x+\xi_1,\ y+\xi_2,\ z+\xi_3)$ in F_T, e.g., $\tilde{R}_{13}\equiv\tilde{R}_{uw}$. δ_{ij} is the Kronecker delta,

$$\xi=\sqrt{\xi_1^2+\xi_2^2+\xi_3^2} \tag{24}$$

$$\zeta=\xi/1.339L_u^x \tag{25}$$

and $f(\zeta)$ and $g(\zeta)$ are the longitudinal and lateral correlation coefficients, respectively.

This model can be applied to situations involving a uniform mean flow $\bar{U}$ where time domain measurements are taken and time delays included by making use of the frozen flow assumption. If the axes are so oriented that the mean flow $\bar{U}$ is the positive x direction, then ξ_1 must be replaced by $(\Delta x-\bar{U}\tau)$ where τ is the time dealy applied to the measurement at (xyz) and Δx represents the probe separation in the x direction and follows the same sign convention as ξ_1. In the case of measurements made along a glide slope of γ_E aligned into a uniform mean flow $\bar{U}$, taking (xyz) as the upper probe location and $(x+\xi_1,\ y+\xi_2,\ z+\xi_3)$ as the lower probe location, one requires [where $\tau=t_2-t_1$ as in Eq. (19)]

$$\begin{aligned}\xi_1&=(h_2-h_1)/\tan\gamma_E-\bar{U}(t_2-t_1)\\ \xi_2&=0\\ \xi_3&=h_2-h_1\end{aligned} \tag{26}$$

and

$$\tilde{\mathfrak{R}}(t_1,t_2)=\tilde{R}(\xi_1,\xi_2,\xi_3) \tag{27}$$

where h_1 and h_2 are the heights above ground level of the upper and lower probes, respectively, and t_1 and t_2 are the times at which the aircraft reaches these locations.

When attempting to apply the above formulation to situations involving wind shear, a problem arises. If it is assumed that the flow is frozen in horizontal layers and that

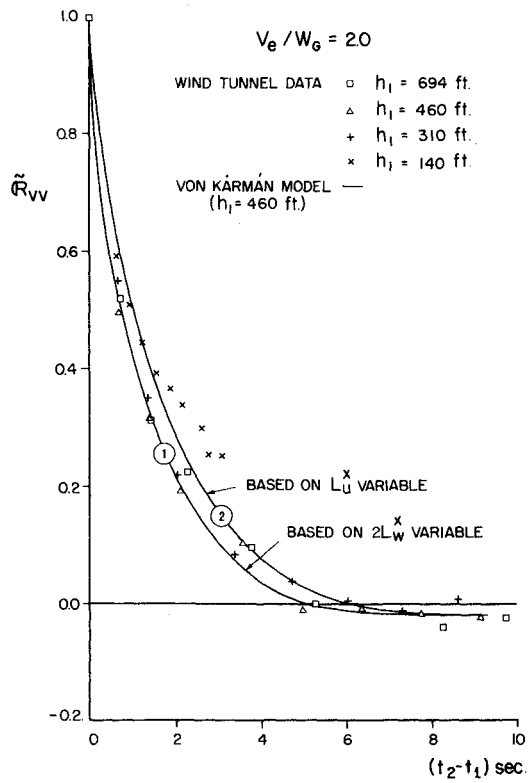

Fig. 6 Turbulence correlation $\tilde{R}_{vv}$.

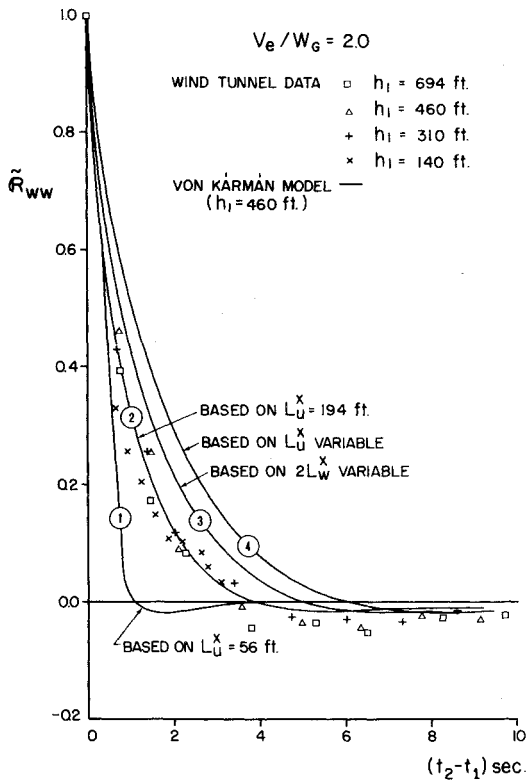

Fig. 7 Turbulence correlation $\tilde{R}_{ww}$.

each layer is traveling at the local mean wind speed, then the spatial organization among the turbulence components becomes a function of time. This loss in spatial organization results from the various layers slipping over one another such that a fixed time delay between the signals from two velocity probes at different levels in the flow no longer corresponds to a single fixed spatial separation in the flowfield. Thus, in applying this model, one is in effect trying to describe the

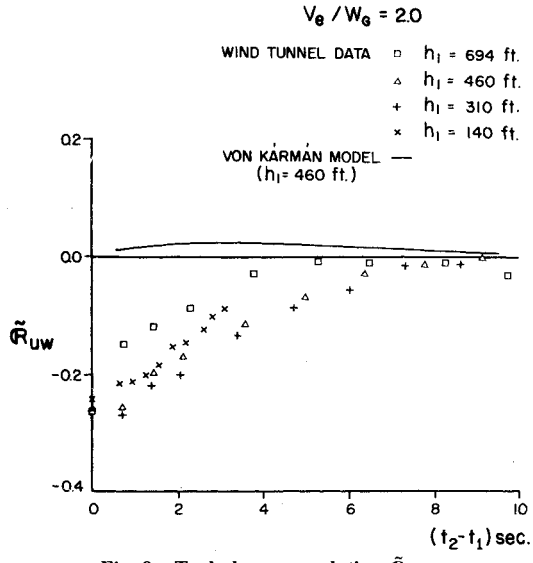

Fig. 8 Turbulence correlation $\tilde{R}_{uw}$.

results found for a limited spatial separation in a shear flow by the best fit equivalent homogeneous, isotropic, Gaussian, frozen flow results. To the extent that the physical probe separations employed spanned only a portion of the shear layer before $\tilde{R}$ became negligibly small (and only modest ranges in $\bar{U}$ and L_u^x were encountered) it seems reasonable to assume that the dominant features of the flowfield in a particular measurement region could be fitted by such a model.

In order to evaluate the above model formulation for $\tilde{R}(t_1,t_2)$, respresentative values for $\bar{U}$ and L_u^x must be selected for each pair of velocity probe locations. It is found that varying $\bar{U}$ and L_u^x affects the shape of the curves for the diagonal elements of $\tilde{R}$ to the greatest extent in the mid range. Increasing L_u^x and decreasing $\bar{U}$ results in an increasing $\tilde{R}_{ii}$ in this region.

In comparing the model with the wind tunnel turbulence correlation measurements it was found that if the values of $\bar{U}$ and L_u^x were restricted to lie between those found at the upper and lower probe locations, then taking values of $\bar{U}=W$ and L_u^x corresponding to the lower probe location produced (marginally) the best agreement. (For full details see Ref. 5.) When this computation is carried out for $\tilde{R}_{uu}$ with $V_e/W_G=1.5$, the results are as shown in Fig. 4 for three values of h_l, the height of the upper probe above ground level. It is seen that the spread in the model results for various values of h_l is similar in magnitude to the spread in twind-tunnel data. However, the trends with increasing h_l do not agree. Whereas the wind-tunnel data tend to collapse onto a single curve (except for the results at $h_l=140$ ft which tend to lie slightly above the rest), the model results show a small but noticeable reduction in $\tilde{R}_{uu}$ with decreasing values of h_l. Similar trends were found for the remaining diagonal elements of $\tilde{R}$.

As a compromise solution it was decided to find a single model curve that would best represent the complete set of wind-tunnel-derived $\tilde{R}_{uu}$ data and ignore the spread in the data at the lowest h_l values. (The impact of this simplification on predicted aircraft response will be checked in the next section.) As seen from Fig. 4, the model curve for $h_l=460$ ft was found to be most suitable. Since these data represent conditions near the middle of the boundary layer, it seemed to be a representative choice. Similar results were achieved for the speed ratio $V_e/W_G=2.0$. Curve 2 in Figs. 5 and 6 shows the acceptable fits achieved for $\tilde{R}_{uu}$ and $\tilde{R}_{vv}$ by using model results for $h_l=460$ ft.

When the $\tilde{R}_{ww}$ data were examined, a problem arose. Due to the small values of ξ_3 generated for $\gamma_E=15$ deg, the model

predicts $\tilde{\mathcal{R}}_{ww} \approx \tilde{\mathcal{R}}_{vv}$ for the present case. Since the wind-tunnel-generated $\tilde{\mathcal{R}}_{ww}$ data have their zero crossing at smaller values of $(t_2 - t_1)$ than the corresponding $\tilde{\mathcal{R}}_{vv}$ results, the initial model fit for $\tilde{\mathcal{R}}_{ww}$ was poor (see the model results based on curve 4 in Fig. 7). A partial answer to this problem was found when the lateral turbulence scale L_w^x was examined in the region in which these measurements were taken. Whereas the theory behind the von Kármán model predicted that $L_u^x = 2L_w^x$, it was found that this was not generally true in our wind tunnel flowfield (see Fig. 3). For example, at $h_1 = 460$ ft, $L_u^x = 356$ ft and $2L_w^x = 272$ ft. When $2L_w^x$ was used instead of L_u^x in the model, slightly better agreement with the $\tilde{\mathcal{R}}_{ww}$ experimental results was achieved (see the model results based on curve 3 in Fig. 7). An acceptable fit to the other lateral correlation $\tilde{\mathcal{R}}_{vv}$ was also achieved using $2L_w^x$ as shown by curve 1 in Fig. 6. [It was found that the best model fit to the $\tilde{\mathcal{R}}_{ww}$ wind tunnel data was achieved by using a constant value of $L_u^x = 194$ ft (see curve 2 in Fig. 7).]

The application of this model to the off-diagonal elements of $\tilde{\mathcal{R}}$ was not successful. Figure 8 shows the fit achieved for $\tilde{\mathcal{R}}_{uw}$. The trends in the experimental data are not predicted by the model. The importance of $\tilde{\mathcal{R}}_{uw}$ in estimating the rms response of an aircraft to turbulence in the landing approach will be determined in the next section.

Computation of a STOL Aircraft's Response to Turbulence During Landing Approach

In this section, the turbulence correlation technique is used to predict the longitudinal response to turbulence during the landing approach of a light STOL transport. These results will be used to indicate the form of the solutions obtained and to demonstrate the sensitivity of the dispersion estimates to off-diagonal elements of $\tilde{\mathcal{R}}$ and the von Kármán model.

The aircraft was taken to be the twin-engined, turbo-prop, light STOL transport (11,000 lb) whose properties are outlined in Refs. 4, 5, and 7. The reference equilibrium flight condition was a constant airspeed landing approach along a rectilinear glide slope in the presence of a constant headwind. This study has considered only the case of fixed controls. No closed-loop control due to a pilot or autopilot has been included. Although the resulting open-loop analysis does not predict aircraft response levels found during a normal closed-loop landing approach, it is felt that it is sufficient for the present purposes of demonstration and comparison. In fact an open-loop analysis is expected to be more responsive to changes in the turbulence model and thus should produce a more sensitive test of turbulence-model-induced effects. Response due to wind shear and initial conditions are not presented here (see Ref. 4 for a treatment of these effects).

Table 1 STOL aircraft characteristics[a]

V_e/W_G	1.5	2.0
C_{L_e}	2.219	1.257
C_{D_e}	0.397	0.292
C_{T_e}	0.145	0.103
ω_{sp} (rad/s)	1.944	2.572
ζ_{sp}	0.655	0.651
$T_{1/2_{sp}}$ (s)	0.544	0.414
ω_{ph} (rad/s)	0.392	0.297
ζ_{ph}	0.132	0.206
$T_{1/2_{ph}}$ (s)	13.444	11.333

[a] ω = undamped natural frequency, ζ = damping ratio, $T_{1/2}$ = time to half amplitude, $(\ )_{sp}$ = short period, $(\ )_{ph}$ = phugoid.

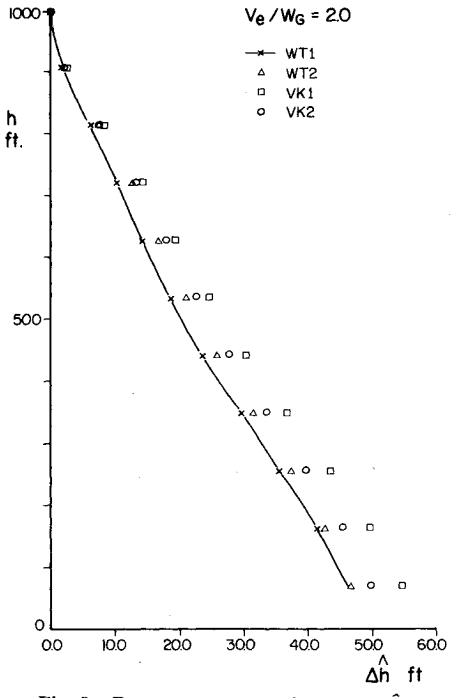

Fig. 9 Rms response to turbulence, $\Delta\hat{h}$.

The mean wind profile is given by Eq. (22) with $W_G = 66$ fps and $h_G = 1000$ ft. The following parameters complete the specification of the flight condition: $\gamma_E = 15$ deg, $V_e/W_G = 1.5$, 2.0, and $W_e = 57$ fps. The aircraft characteristics corresponding to those two reference equilibria are given in Table 1. Also, since only the longitudinal response is to be studied, only $\mathcal{R}_{uu}$, $\mathcal{R}_{ww}$, $\mathcal{R}_{uw}$, and $\mathcal{R}_{wu}$ need be employed.

The expected rms value of the state vector (Eq. 5) has been computed as a function of height for a number of conditions in order to study the influence of various factors on the predicted aircraft response due to turbulence. These computations begin at $h = 1000$ ft (where the rms response is taken to be zero) and are terminated at $h = 69$ ft. Two sources of $\mathcal{R}$ data have beem employed. One is the set of wind tunnel measurements, the other is the modified von Kármán model.

In the present study, the modified von Kármán model was employed by finding suitable single-model curves to represent the measured $\tilde{R}_{uu}$ and $\tilde{R}_{ww}$ data sets. A complete set of model $\tilde{R}_{uu}$ and $\tilde{R}_{ww}$ data was then computed for all the probe-pair locations employed in the wind tunnel measurement program by picking off the appropriate quantity from these single curves at the particular values of $(t_2 - t_1)$ corresponding to these probe locations. $\tilde{R}_{uw}$ and $\tilde{R}_{wu}$ were taken as zero. The nondimensional model $\tilde{\mathcal{R}}$ data were then dimensionalized by employing the product of the appropriate rms turbulence values.

Two data sets based on the modified von Kármán model were generated and designated VK1 and VK2. VK1 employed a single curve to represent the $\tilde{R}_{uu}$ data and was based on wind tunnel measurements of L_u^x and W for $h_1 = 460$ ft. These parameters were taken as the values at the lower probe location (see curve 2 of Fig. 5). The single-model curve for $\tilde{R}_{ww}$ was found in a similar manner but employed a turbulence

Table 2 Percent difference between WT1 and WT2 rms results 100 (WT2 – WT1)/WT1

h, ft	$\Delta\hat{u}$	$\Delta\hat{w}$	$\Delta\hat{q}$	$\Delta\hat{\theta}$	$\Delta\hat{x}_1$	$\Delta\hat{h}$
1000	0	0	0	0	0	0
530	2.3	−1.7	−3.4	−5.8	−2.7	13.5
69	−1.8	−4.3	−6.1	−7.8	−2.1	0.4

Table 3 Percent difference between WT1 and VK1 rms results 100 (VK1 – WT1)/WT1

h, ft	$\Delta\hat{u}$	$\Delta\hat{w}$	$\Delta\hat{q}$	$\Delta\hat{\theta}$	$\Delta\hat{x}_I$	$\Delta\hat{h}$
1000	0	0	0	0	0	0
530	2.5	−10.6	−9.2	−4.8	0	33.0
69	1.2	−21.1	−14.6	−4.1	0.7	18.4

Table 4 Percent difference between WT1 and VK2 rms results 100 (VK2 – WT1)/WT1

h, ft	$\Delta\hat{u}$	$\Delta\hat{w}$	$\Delta\hat{q}$	$\Delta\hat{\theta}$	$\Delta\hat{x}_I$	$\Delta\hat{h}$
1000	0	0	0	0	0	0
530	1.5	−1.7	−2.4	−5.6	−0.3	22.2
69	0.5	−15.2	−10.5	−4.9	4.6	8.0

Table 5 Model correlation data sets

Model data set	$\tilde{\mathfrak{R}}_{uu}$ curve (Fig. 5)	$\tilde{\mathfrak{R}}_{ww}$ curve (Fig. 7)
VK1	2	3
VK2	2	2
VK3	1	2
VK4	3	2
VK5	2	1
VK6	2	4

scale based on measured values of $2L_w^x$ (see curve 3 of Fig. 7). VK2 employed the same $\tilde{R}_{uu}$ as VK1. However, in this case the representation of $\tilde{R}_{ww}$ was accomplished by fitting a curve to the wind tunnel measurements (see curve 2 of Fig. 7). In practice, model VK1 would be easier to apply because it is based on an algorithm that does not require the measurement of $\tilde{\mathfrak{R}}$ whereas VK2 would require the measurement of $\tilde{R}_{ww}$ at the midpoint of the boundary layer.

Two data sets based on wind tunnel measurements were generated – WT1 and WT2. WT1 employed a wind tunnel measurements of R_{uu}, R_{ww}, R_{uw}, and R_{wu} while WT2 employed the wind tunnel measurements of R_{uu} and R_{ww}, where $R_{uw} = R_{wu} = 0$.

Figure 9 shows an example of the growth in the rms response as the landing approach is continued. The solid line represents the results for the WT1 data and the open triangles those for WT2 (i.e., the case with $R_{uw} = R_{wu} = 0$). By comparing these two data sets, it is possible to determine the importance of including the terms R_{uw} and R_{wu} in computing the longitudinal rms response to turbulence of light STOL transports. Figure 9 represents the state variable most affected by these terms. Table 2 gives the percent change in the predicted rms response caused by dropping R_{uw} and R_{wu} for several points along the landing approach. If agreement within 10% is taken to be a reasonable limit (one compatible with current precision standards for employing numerical techniques to predict the rms response based on an experimentally measured $\mathfrak{R}$ matrix), then it is seen that only one estimate ($\Delta\hat{h}$) lies (marginally) outside this criterion. From this it can be predicted that the dropping of R_{uw} and R_{wu} is probably a reasonable simplification in estimating the longitudinal rms response of the present class of aircraft. Similar trends were found for computations made for the speed ratio $V_e/W_G = 1.5$. In the present study, no detailed analysis of the influence of the off-diagonal elements of the $\mathfrak{R}$ matrix on the off-diagonal elements of the state variable covariance matrix was carried out, although it was noted that some of these elements were strongly influenced by the dropping of R_{uw} and R_{wu}.

The results achieved using model data sets of VK1 and VK2 are also shown in Fig. 9. The percent difference between these model results and those for data set WT1 (the complete wind tunnel data set) is given in Tables 3 and 4. Again it is found

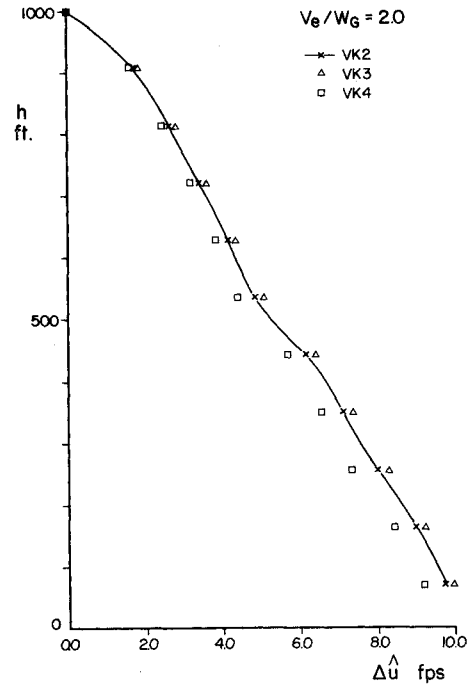

Fig. 10 Rms response to turbulence, $\Delta\hat{u}$.

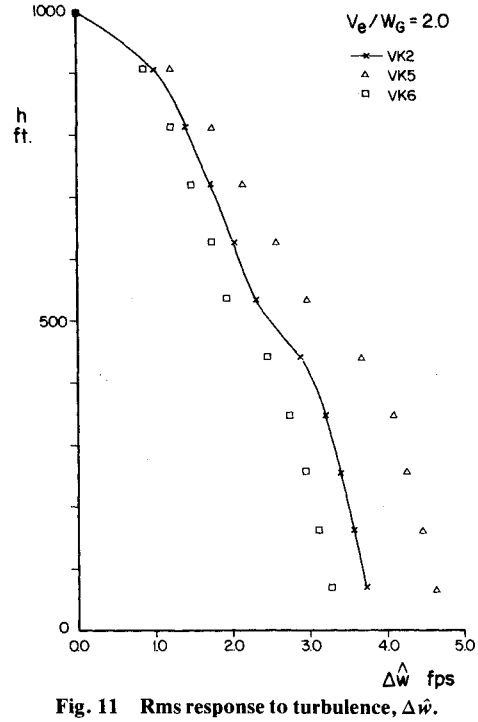

Fig. 11 Rms response to turbulence, $\Delta\hat{w}$.

that the poorest match is achieved for the $\Delta\hat{h}$ estimates. Agreement between the model-response predictions and those of the full wind tunnel set WT1 is better than 6% for state variables Δu, $\Delta\theta$, and Δx_I, whereas agreements in the order of 20% are found for Δw, Δq, and Δh. VK2, having a better representation of the $\tilde{R}_{ww}$ data from the wind tunnel, gave slightly better results on the average than VK1. The plots of Figs. 5 and 7 suggest that an alternative approach to that used in VK2 would be to employ the actual wind tunnel measurements of $\tilde{R}_{uu}$ and $\tilde{R}_{ww}$ for $h_I = 460$ ft as the single curves that form the model base. While this would not remove the need for correlation measurements, it would greatly reduce the time needed for experimental measurements. One would expect the agreement with the WT1 results to be similar to that found for VK2.

In order to obtain an estimate of the sensitivity of the predicted aircraft response to changes in the shapes of $\tilde{\mathfrak{R}}_{uu}$ and $\tilde{\mathfrak{R}}_{ww}$, several model data sets were generated based on the curves of Figs. 5 and 7. These additional data sets are designated VK3 through VK6 and are based on the pairs of single curves outlined in Table 5 (VK1 and VK2 are included for completeness).

Typical comparisons among the most affected rms response predictions for the various cases are given in Fig. 10 (the influence of $\tilde{\mathfrak{R}}_{uu}$ on $\Delta\hat{u}$) and in Fig. 11 (the influence of $\tilde{\mathfrak{R}}_{ww}$ on $\Delta\hat{w}$). It was generally found that the shape of $\tilde{\mathfrak{R}}_{uu}$ had the greatest impact on $\Delta\hat{u}$, $\Delta\hat{\theta}$, $\Delta\hat{x}_I$, and $\Delta\hat{h}$ and a negligible effect on $\Delta\hat{w}$ and $\Delta\hat{q}$. $\tilde{\mathfrak{R}}_{ww}$ was found to have the greatest effect on $\Delta\hat{w}$, $\Delta\hat{q}$, and $\Delta\hat{h}$ with a negligible effect on $\Delta\hat{u}$, $\Delta\hat{\theta}$, and $\Delta\hat{x}_I$. It appears that the response computations are moderately sensitive to changes in $\tilde{\mathfrak{R}}_{uu}$ and $\tilde{\mathfrak{R}}_{ww}$.

Conclusions

The conclusions reported below must be interpreted taking into account the particular set of conditions under which the present study was conducted. However, a comparison of the $\tilde{\mathfrak{R}}$ data employed in the present study with similar data for steeper glide slopes and other boundary-layer profiles,[5] indicates that the proposed technique for employing the modified von Kármán model should have fairly general application in cases involving boundary layers over uniform terrain. Other conclusions, dependent upon the aircraft configuration, presently must be considered applicable only to the class of vehicle represented by the study aircraft. The conclusions follow:

1) The flight path correlation technique can be successfully applied to determine the rms response of an aircraft to turbulence encountered during the landing approach.

2) Single curves can be used to represent the significant features of the diagonal elements in the $\tilde{\mathfrak{R}}$ matrix. These single curves can be generated by using a modified von Kármán model.

3) Knowledge of the off-diagonal elements in the $\tilde{\mathfrak{R}}$ matrix is not essential in estimating the longitudinal rms response of an aircraft to turbulence in the planetary boundary layer.

4) Reasonably precise estimates of the rms response of some important state variables (e.g., $\Delta\hat{w}$ or $\Delta\hat{\alpha}=\Delta\hat{w}/V_e$ and $\Delta\hat{h}$) can only be achieved by employing a complete grid of measured values of $\tilde{\mathfrak{R}}$. This approach will also be required if local nonuniform terrain features or buildings influence the planetary boundary layer.

5) If $\tilde{\mathfrak{R}}$ measurements are not available, a model based on von Kármán's theory can be applied with some success, in computating aircraft response. In this case, data on turbulence levels, turbulence scale, and wind profile are required.

Acknowledgment

This research has been supported by the Air Force Flight Dynamics Laboratory, Wright-Patterson Air Force Base, Ohio, and the National Research Council of Canada.

References

[1] Etkin, B. and Teunissen, H. W., "A Method for the Estimation of Flight Path Perturbation During Steep Descents of V/STOL Aircraft," *Canadian Aeronautics and Space Institute Transactions*, Vol. 7, Sept. 1974, pp. 60-68.

[2] Cunningham, T. B. and Swaim, R. L., "Design of a Manual Control System for a STOL Aircraft on Microwave Landing System Curved Approaches," *Proceedings of the Tenth Annual Conference on Manual Control*, Wright-Patterson Air Force Base, Ohio, 1974, pp. 641-666.

[3] Gerlach, O. H., van de Moesdijk, G.A.J., and van der Vaart, J. C., "Progress in the Mathematical Modelling of Flight in Turbulence," *Flight in Turbulence*, AGARD CP-140, 1973, pp. (5-1)-(5-38).

[4] Reid, L. D., Markov, A. B., and Graf, W. O., "The Application of Techniques for Predicting STOL Aircraft Response to Wind Shear and Turbulence During the Landing Approach," University of Toronto, UTIAS Report No. 215, June 1977.

[5] Reid, L. D., Etkin, B., Teunissen, H. W., and Hughes, P. C., "A Laboratory Investigation Into Flight Path Perturbations During Steep Descents of V/STOL Aircraft," AFFDL-TR-76-84, Aug. 1976.

[6] Etkin, B., *Dynamics of Atmospheric Flight*, Wiley, New York, 1972, pp. 121-195 and 529-563.

[7] Reeves, P. M., Campbell, G. S., Ganzer, V. M., and Joppa, R. G., "Development and Application of a Non-Gaussian Atmospheric Turbulence Model for Use in Flight Simulators," NASA CR-2451, Sept. 1974.